Supporting Information

Synthesis of 2-Imidazolidinone from Ethylenediamine using CO_2 as a C1 building block over the SnO_2/g-C_3N_4 catalyst

Akash Mandal,[a] Sumanta Mondal,[b] Aniruddha Singha,[a] Akash Surajlal Rane,[a] Sourav Ghosh,[c] Ranjit Thapa,[c,d] Asim Bhaumik,*[b] and Biswajit Chowdhury*[a]

[a] Department of Chemistry and Chemical Biology, Indian Institute of Technology (ISM) Dhanbad, Dhanbad, Jharkhand 826004, India. E-mail: *biswajit72@iitism.ac.in*

[b] School of Materials Sciences, Indian Association for the Cultivation of Science, Jadavpur, Kolkata 700032, India. E-mail: msab@iacs.res.in

[c]Department of Physics, SRM University–AP, Amaravati 522 240, Andhra Pradesh, India.

[d]Centre for Computational and Integrative Sciences, SRM University–AP, Amaravati 522 240, Andhra Pradesh, India.

*Corresponding author. *Email: biswajit72@iitism.ac.in*

Contents.

1. **Experimental section**
2. **Characterization techniques.**
3. **Computational Details.**
4. **Figure S1.** PXRD pattern of 10 SnO_2/g-C_3N_4 catalyst.
5. **Figure S2**. FT-IR spectrum of SnO_2, g-C_3N_4 and 5, 10, and 15 SnO_2/ g-C_3N_4 catalyst.
6. **Fig. S3** (a, b) TEM, (c) HRTEM, and (d) SAED pattern of the 10 SnO_2/g-C_3N_4 catalyst.
7. **Figure S4** EDS spectra of 10 SnO_2/g-C_3N_4 catalyst.
8. **Figure S5** Elemental mapping image (a-f) of 10 SnO_2/g-C_3N_4 catalyst.
9. **Figure S6** XPS spectra of synthesized SnO_2, and 10 SnO_2/g-C_3N_4 catalyst: (a,b) survey spectrum, (c,d) Sn 3d, and (e,f) O 1s spectrum.
10. **Table S1**. XPS result of SnO_2 and 10 SnO_2/g-C_3N_4 catalyst.
11. **TGA analysis.**
12. **Figure S7** TGA curve of pure SnO_2, g-C_3N_4, and 10 SnO_2/g-C_3N_4 materials.
13. **Figure S8** N_2-physisorption isotherm and pore size distribution curve of 10 SnO_2/g-C_3N_4 composite.
14. **Catalytic activity test.**
15. **Figure S9** GC-MS chromatogram of the reaction mixture after 2 h.
16. **Figure S10** Mass spectra of 2-imidazolidinone confirmed by GC-MS analysis.
17. **Table S2:** Reaction of different substrate [a]
18. **Figure S11** Effect of different reaction parameters on the conversion of ethylenediamine to 2-imidazolidinone over 10 SnO_2/g-C_3N_4.
19. **Reusability test.**
20. **Figure S12** The reusability test of the 10 SnO_2/g-C_3N_4 catalyst.
21. **Figure S13** PXRD patterns of the 10 SnO_2/g-C_3N_4 before and after 4th cycle.
22. **Figure S14** TEM, HRTEM and SAED pattern of 10 SnO_2/g-C_3N_4 fresh and spent catalyst after 4th cycle.
23. **Figure S 15** XPS spectra of the 10 SnO_2/g-C_3N_4 fresh and spent catalyst after 4th cycle.
24. **Figure S16** FTIR spectra of the 10 SnO_2/g-C_3N_4 fresh and spent catalyst after 4th cycle.
25. **Figure S17** (a) Charges on atoms in the topmost surface layer and (b) charge density difference on the SnO_2/g-C_3N_4 surface.
26. **Table S3** Comparison results of synthesis of ethylene urea (EU) from ethylenediamine (EDA) and ethylenediamine carbamate (EDA-CA).
27. **References.**

Experimental section

Chemicals

Stannic Chloride Anhydrous (SRL chemicals India), Methanol (Finar), Ammonia Solution (Qualigens), Melamine (Alfa Aesar), ethylenediamine (Alfa Aesar), ethanolamine (Loba Chemie Pvt. Ltd.), tridecane (TCI).

Synthesis of SnO_2 nanoparticles

Nanocrystalline tin oxide SnO_2 has been prepared by the conventional precipitation method.[1] 2.602 g (10 mmol) of anhydrous stannic chloride is dissolved in 100 ml of methanol and continued the stirring for 15 minute to dissolve it completely. It was followed by dropwise addition of ammonia solution $NH_3.H_2O$ to alc. solution of tin chloride at room temperature. Then we adjust the pH of the mixed solution to 8 and obtained a white precipitate of tin oxide. The solution was remained still for 1 hour with continuous stirring. The obtained product was taken for centrifugation and washed with methanol and deionised water several times to remove chloride ions coming from stannic chloride. The resulting product was dried at 100 °C for 24 h in drying oven and calcined in muffle furnace at 400°C temperature for 4 h.

Synthesis of g-C_3N_4

The g-C_3N_4 was obtained by directly heating the melamine (nitrogen-rich organic compound). Melamine (6 g) was placed in porcelain crucible and calcined it at 550°C in muffle furnace for 4 h with the heating rate of 5°C/min. The calcined product was then grinded in mortar and pestle, a pale-yellow colour powdered g-C_3N_4 obtained.[2]

Synthesis of SnO_2/g-C_3N_4 nanocomposites

Different weight percent of SnO_2 used for synthesizing the catalyst, like 5 wt. %, 10 wt. %, 15 wt. % of SnO_2, and impregnated it with g-C_3N_4 in distilled water. A 10 wt. % SnO_2/g-C_3N_4 catalyst have been prepared by taking 0.1 g SnO_2 powder and impregnating it with 1 g of g-C_3N_4, both dissolved in 25 ml of distilled water in a 100 ml beaker. A resulting mixture was stirred and heating simultaneously at 100 °C till the water gets evaporated completely. Then the beaker was kept inside the hot oven at 100 °C for a day, so that the catalyst is completely moisture free. The obtained powder was grinded properly to fine powder form.

Synthesis of in-situ SnO_2/g-C_3N_4 Composite

In a 100 mL beaker, 0.219 g of anhydrous stannic chloride was dissolved in 10 mL of methanol under continuous stirring. Separately, 0.9 g of as-prepared g-C_3N_4 was dispersed in 25 mL of deionized water and stirred for 30 min. The stannic chloride solution was then added dropwise to the g-C_3N_4 dispersion, followed by a further 30 min of stirring. Subsequently, ammonia solution ($NH_3 \cdot H_2O$) was added dropwise to adjust the pH to 8, and the mixture was stirred for an additional 2 h to facilitate precipitation. The resulting solid was collected by centrifugation, thoroughly washed with deionized water and methanol, and dried overnight at 100 °C. Finally, the product was calcined at 400 °C for 2 h to obtain the SnO_2/g-C_3N_4 composite catalyst.

Characterization techniques:

The crystalline structure of the samples was analyzed using X-ray diffraction (XRD) on a Rigaku SmartLab high-resolution diffractometer (HRXRD) equipped with Cu Kα radiation. The measurements were carried out in the 2θ range of 10°–80°, with a scanning rate of 6° min^{-1} and a step size of 0.02°. Fourier transform infrared (FTIR) spectra of all samples and reaction products were obtained using a PerkinElmer GX spectrometer (USA) within the wavenumber range of 4000–400 cm^{-1}, employing KBr pellet techniques. High-resolution transmission electron microscopy (HRTEM) was conducted on a Talos F200X G2 instrument (Thermo Scientific, USA) operated at 200 kV to study the crystallite size, exposed crystal facets, and morphology. For TEM analysis, the metal oxide powders were dispersed in ethanol and drop-cast onto copper grids, followed by drying. X-ray photoelectron spectroscopy (XPS) measurements were performed using a PHI 5000 Versa Probe III spectrometer (USA) with Al Kα (1486.6 eV) radiation as the excitation source, and the binding energies were calibrated against the C 1s peak at 284.6 eV.[3] Nitrogen adsorption–desorption experiments were conducted using a Micromeritics ASAP 2020 analyzer to determine the surface area, pore volume, and pore size distribution of the samples. Prior to measurements, all samples were degassed under high vacuum at 200 °C for 3 h to eliminate adsorbed gases and moisture. The Brunauer–Emmett–Teller (BET) method was used to calculate the specific surface area (S_{BET}) of the materials. The acid–base characteristics of the samples were analyzed using temperature-programmed desorption of ammonia (NH_3-TPD) and carbon dioxide (CO_2-TPD), conducted on an Altamira AMI-300 Lite instrument. Before the adsorption analysis, the samples were

pretreated under an argon flow (40 mL min^{-1}) at 150 °C for 1 h. After cooling to room temperature, the gas flow was switched to NH_3 or CO_2 (40 mL min^{-1}) for 1 h to allow adsorption. Subsequently, any physisorbed NH_3 or CO_2 was removed by purging with argon at room temperature for 1 h. The desorption step was then carried out in argon (40 mL min^{-1}), heating from room temperature to 600 °C at a rate of 10 °C min^{-1}. Thermogravimetric analysis (TGA) was performed using a PerkinElmer STA 6000 instrument in the temperature range of 25–800 °C under a continuous flow of nitrogen gas. Electron paramagnetic resonance (EPR) analysis was conducted using a JEOL JES-X310 spectrometer at both room temperature and 77 K.

Computational Details:

The surface model was generated by positioning a SnO_2(101) slab on top of a g-C_3N_4 sheet, maintaining an interlayer distance of about 3.4 Å. The final supercell consists of 164 atoms and maintains a lattice mismatch below 5%. This combined configuration, hereafter referred to as surface(*)-was fully relaxed, along with all associated reaction intermediates, using the Quantum ESPRESSO package.[4-6] Exchange–correlation energy correction has been done using the Perdew–Burke–Ernzerhof (PBE) functional within the Generalized Gradient Approximation (GGA).[7] Electronic and ionic convergence thresholds were set to 7.35×10^{-7} Ry (≈10^{-5} eV) and 1×10^{-4} Ry (≈0.001 eV), respectively, and a force tolerance of 7.78×10^{-4} Ry/Bohr (0.02 eV/Å) was applied in all structural optimizations. Brillouin-zone integration was performed using a 3 × 3 × 1 Monkhorst–Pack k-point mesh.[8] Gaussian smearing with a width of 0.01 Ry was used, and long-range dispersion forces were included via the DFT-D3 van der Waals correction with damping.[9,10] A vacuum layer of 16 Å was added along the z-direction to avoid spurious interactions between periodic images.

The Gibbs free energy change (ΔG) for each reaction step was calculated according to:

$$\Delta G = \Delta E + \Delta ZPE - T\Delta S \qquad \text{..... (1)}$$

where ΔE is the DFT-derived energy difference between the adsorbed intermediate and the pristine surface, ΔZPE denotes the zero-point energy correction, and ΔS represents the entropy change of both gas-phase and adsorbed species at 298.15 K.[11,12]

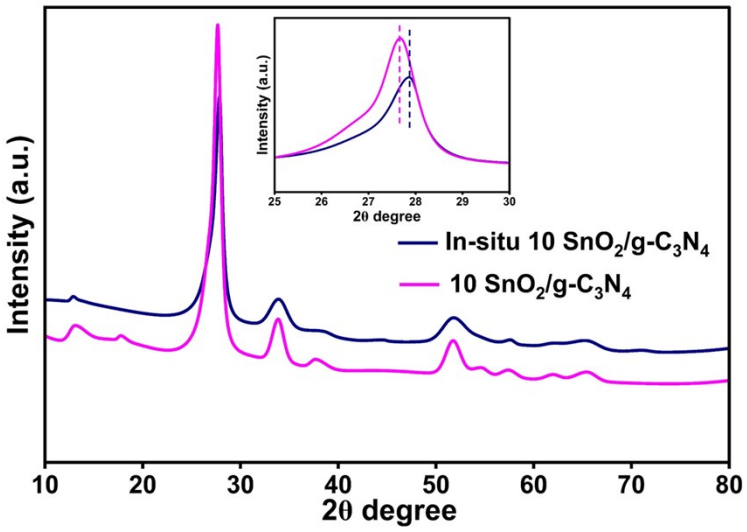

Figure S1. PXRD pattern of 10 SnO_2/g-C_3N_4 catalyst.

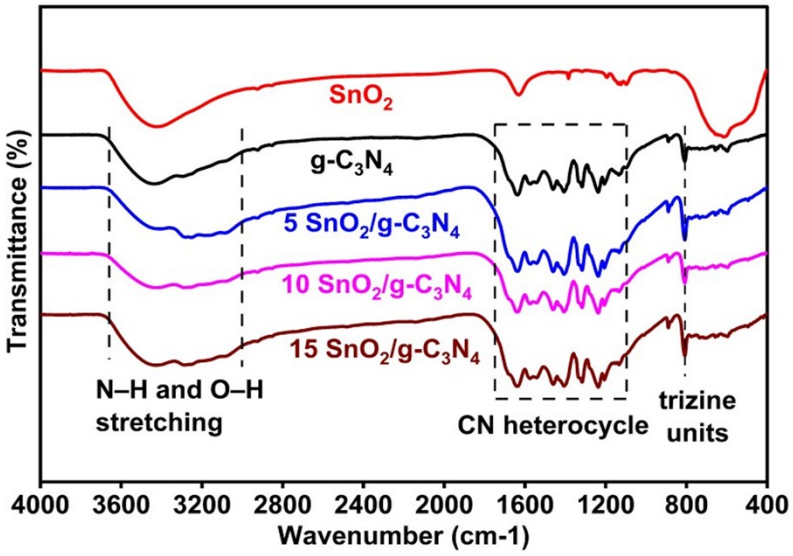

Figure S2. FT-IR spectrum of SnO_2, g-C_3N_4 and 5, 10, and 15 SnO_2/ g-C_3N_4 catalyst.

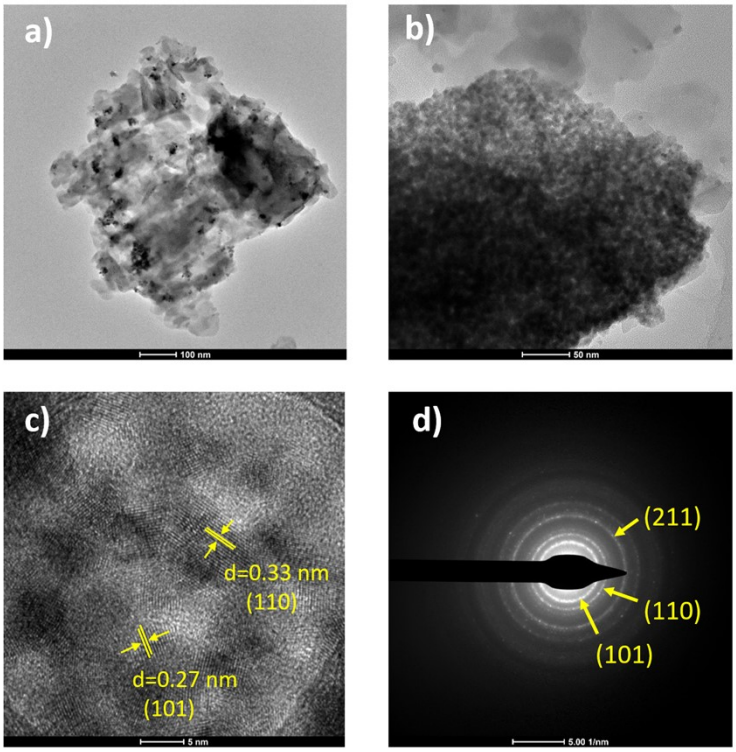

Fig. S3 (a, b) TEM, (c) HRTEM, and (d) SAED pattern of the 10 SnO_2/g-C_3N_4 catalyst.

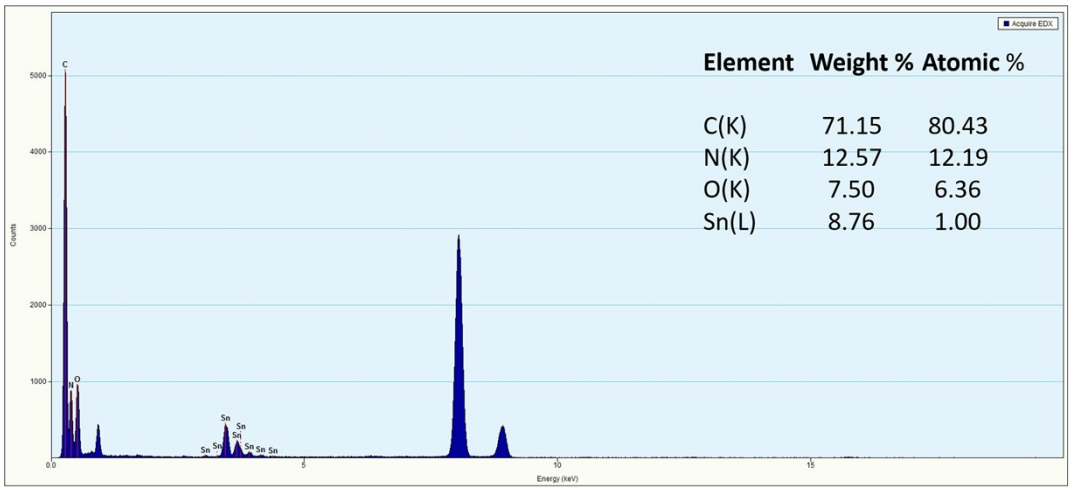

Figure S4 EDS spectra of 10 SnO_2/g-C_3N_4 catalyst.

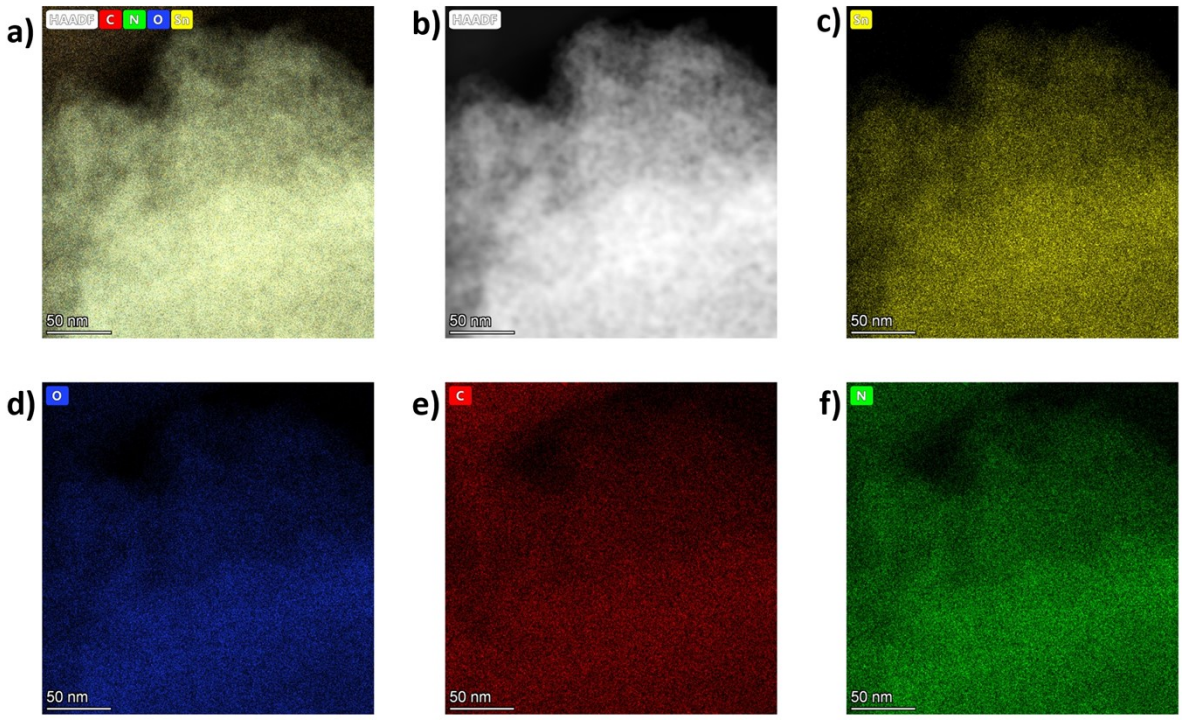

Figure S5 Elemental mapping image (a-f) of 10 SnO_2/g-C_3N_4 catalyst.

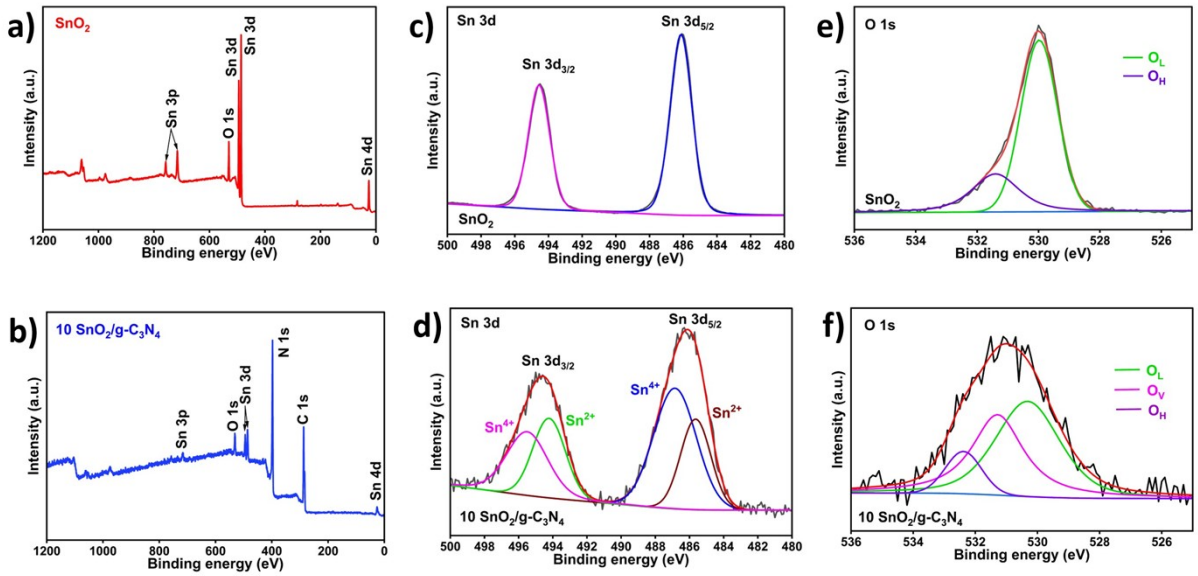

Figure S6 XPS spectra of synthesized SnO_2, and 10 SnO_2/g-C_3N_4 catalyst: (a,b) survey spectrum, (c,d) Sn 3d, and (e,f) O 1s spectrum.

Table S1. XPS result of SnO_2 and 10 SnO_2/g-C_3N_4 catalyst.

Entry	Catalyst	Element orbital	Peak No.	Binding energy (eV)	Assignment
1	SnO_2	Sn 3d	1	486.1	Sn^{4+} ($3d_{5/2}$)
			2	494.5	Sn^{4+} ($3d_{3/2}$)
		O 1s	1	529.9	O_L
			2	531.4	O_H
2	SnO_2/g-C_3N_4	Sn 3d	1	485.6	Sn^{2+} ($3d_{5/2}$)
			2	486.8	Sn^{4+} ($3d_{5/2}$)
			3	494.2	Sn^{2+} ($3d_{3/2}$)
			4	495.5	Sn^{4+} ($3d_{3/2}$)
		O 1s	1	530.3	O_L
			2	531.2	O_V
			3	532.4	O_H

TGA analysis

The thermal stability of SnO_2, g-C_3N_4, and the 10 SnO_2/g-C_3N_4 composite was examined in the 25–800 °C temperature range at a heating rate of 10 °C/min under N_2 atmosphere,[13] and the corresponding TGA profiles are displayed in (**Figure S7**). For g-C_3N_4, no significant mass loss was noticed until about 505 °C. A minor weight decrease was then observed between 520 and 631 °C, which can be ascribed to the initial stages of g-C_3N_4 decomposition. This was followed by a sharp decline in mass from 631 to 760 °C, reflecting the intrinsic thermal instability of g-C_3N_4 in this region. At this stage, the pronounced weight reduction was mainly due to the conversion of g-C_3N_4 into volatile carbon- and nitrogen-based species.[13] Pure SnO_2, in contrast, exhibited almost no weight change throughout the heating cycle, confirming its excellent thermal stability. For the 10 SnO_2/g-C_3N_4 hybrid, weight loss commenced around 502–635 °C, after which a rapid decrease was recorded between 635 and 745 °C. This indicates that the composite is thermally less stable than its individual components, most likely because of SnO_2 crystallization interfering with the layered framework of g-C_3N_4 or the catalytic action of SnO_2 in accelerating g-C_3N_4 decomposition. A similar trend has been reported for ZnO/g-C_3N_4 composites.[14] By approximately 755 °C, the 10SnO_2/g-C_3N_4 material was nearly fully decomposed, evidencing its reduced thermal resistance. Overall, the TGA data (Figure S7) suggest that the composite maintains stability only up to around 500 °C.

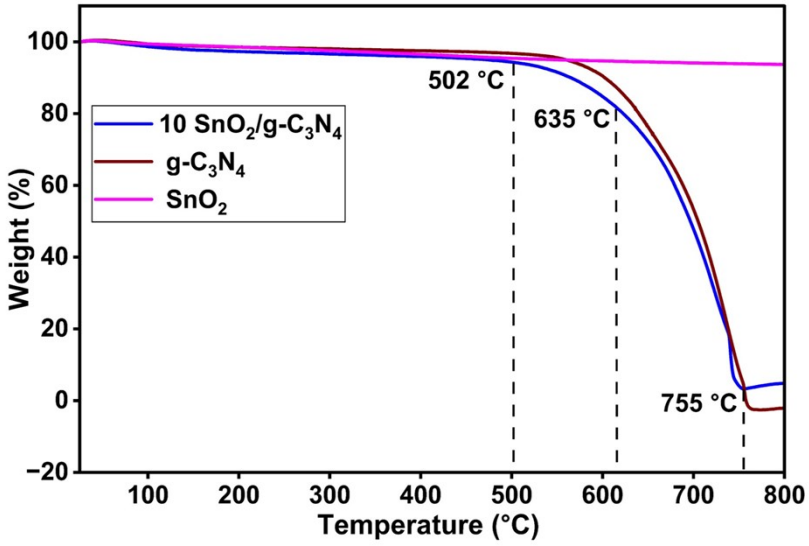

Figure S7 TGA curve of pure SnO_2, g-C_3N_4, and 10 SnO_2/g-C_3N_4 materials.

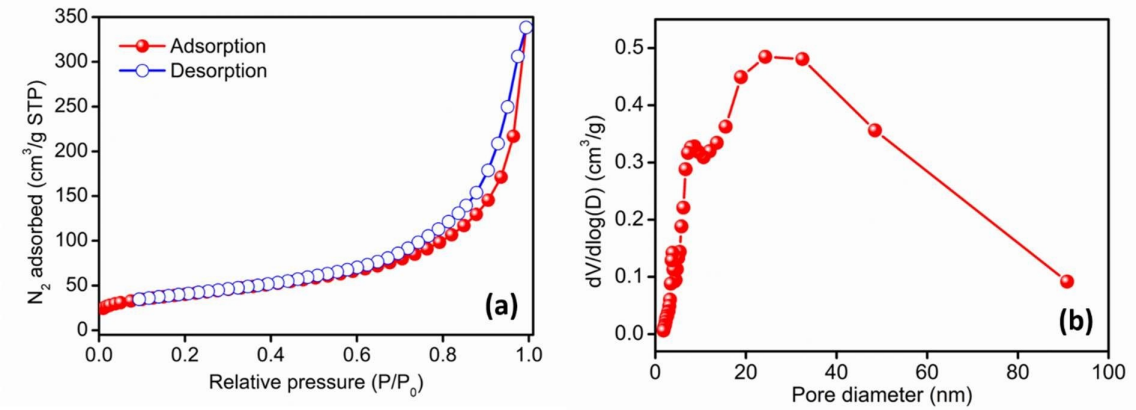

Figure S8 (a) N_2-physisorption isotherm, and (b) pore size distribution curve of 10 SnO_2/g-C_3N_4 composite.

Catalytic activity test

All the reactions executed the in high pressure autoclave reactor with its inner volume of 250 ml. The synthesis of cyclic urea from CO_2 and diamine was as follows: catalyst (250 mg), ethylenediamine (0.1 mol), solvent methanol (80 ml) and internal standard (IS) tridecane (0.1 ml) were together put into autoclave vessel, and then the purging of CO_2 was done (3-4 times). The reactor was then filled with CO_2 to the targeted pressure (2.5 MPa), then we closed the gas line and heated to the desired temperature of the reaction, and constantly stirred at 600 rpm for a fixed time. After the reaction is over, reactor was cooled down to room temperature. The reaction mixture was withdrawn from the vessel, centrifuged, and analyzed using a TRACE 1310 gas chromatograph coupled with an ISQ 7000 single quadrupole mass spectrometer (Thermo Scientific, USA). The conversion of ethylenediamine and selectivity of products were calculated by using tridecane as an internal standard (IS) from eqn. 1 and 2, respectively.[15]

$$\text{Conversion (\%)} = \{(C_0 - C_f)/C_0\} \times 100 \quad (1)$$

$$\text{Selectivity (\%)} = \{C_p/(C_0 - C_f)\} \times 100 \quad (2)$$

(where, C_0 is initial concentration of ethylenediamine, C_f and C_p are concentration of ethylenediamine and the product after the reaction, respectively).

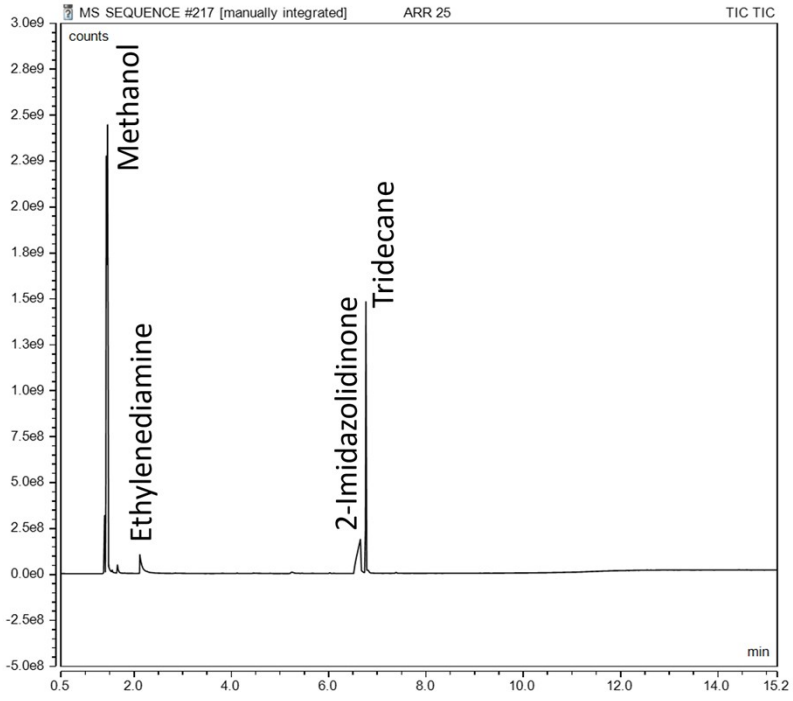

Figure S9 GC-MS chromatogram of the reaction mixture after 2 h.

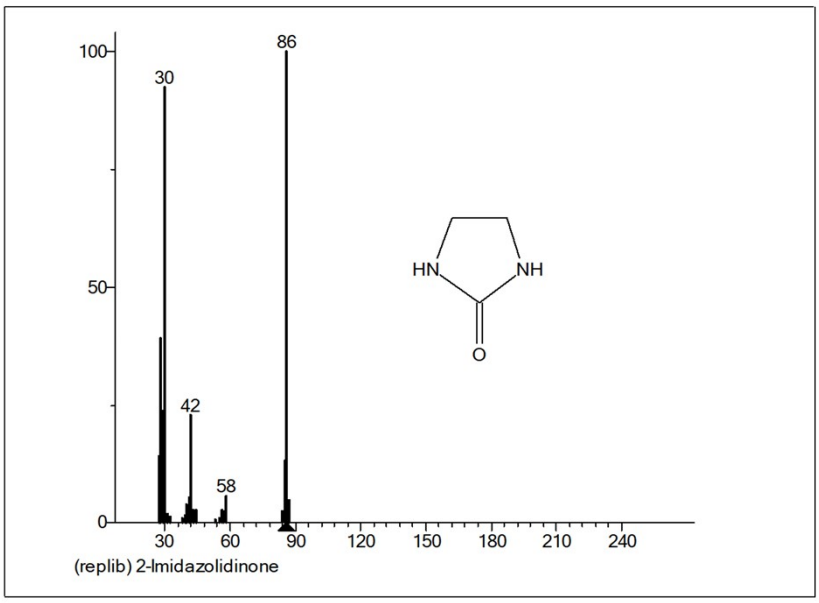

Figure S10 Mass spectra of 2-imidazolidinone confirmed by GC-MS analysis.

Table S2: Reaction of different substrate [a]

Entry	Catalyst	Reactant	Solvent	Conv.[b] (%)	Product	Sel.[c] (%)	Yield
1	10 SnO_2/g-C_3N_4	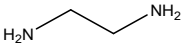	Methanol	95	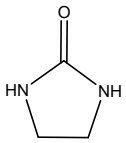	99	94
2	10 SnO_2/g-C_3N_4	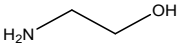	Methanol	16	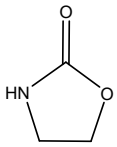	96	15
			Propan-2-ol	83		96	80

[a]Reaction condition: reactant, (0.1 mol); catalyst, (0.2 g); solvent, (80 ml); temperature, (160° C); time, (2 h); CO_2, (2.5 MPa).

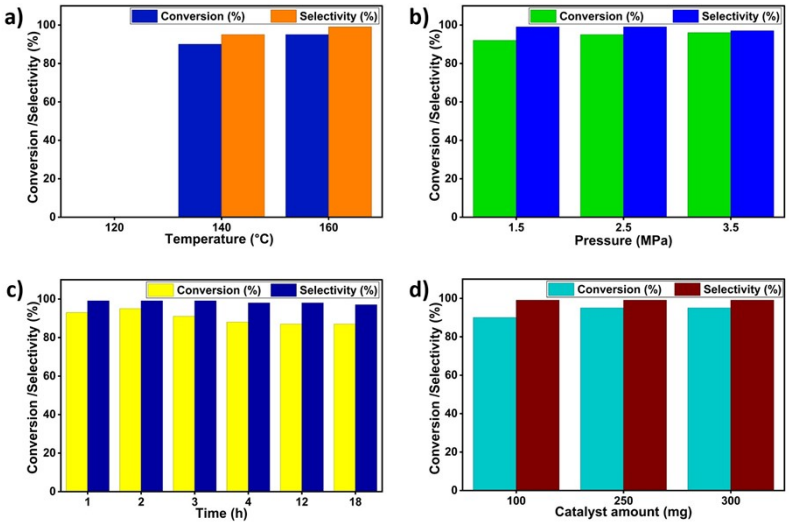

Figure S11 Effect of different reaction parameters on the conversion of ethylenediamine to 2-imidazolidinone over 10 SnO_2/g-C_3N_4: (a) reaction temperature, (b) CO_2 pressure, (c) time, and (d) catalyst amount. Optimized conditions: EDA, 0.1 mol; catalyst, 250 mg; Methanol, 80 ml; tridecane (IS), 0.1 mL; temperature, 160 °C; CO_2 pressure, 2.5 MPa; reaction time, 2 h. During each study, only the parameter of interest was varied while the others were kept constant.

Reusability test

To evaluate the reusability of the catalyst, the spent 10 SnO_2/g-C_3N_4 was recovered after each reaction cycle by centrifugation, thoroughly washed with distilled water to remove residual organics, and dried at 120 °C for 24 h. The recovered catalyst was then reused directly in subsequent reactions without any further treatment. As shown in (**Figure S12**), the catalyst consistently maintained high catalytic activity and yield even after four consecutive cycles. No significant change in conversion or yield was observed, confirming its excellent stability and reusability in the synthesis of cyclic urea. These results highlight the catalyst's robust performance and potential for sustainable catalytic applications.

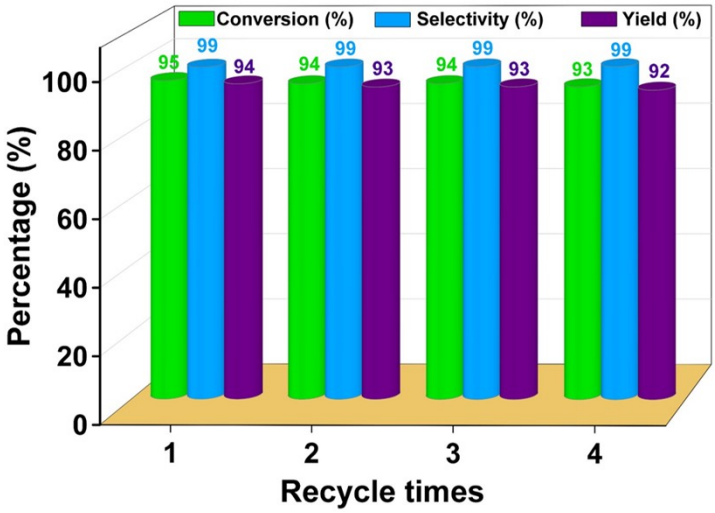

Figure S12 The reusability test of the 10 SnO_2/g-C_3N_4 catalyst. Reaction conditions: EDA, 0.1 mol; catalyst, 250 mg; tridecane (IS), 0.1 mL; 160 °C; CO_2 pressure, 2.5 MPa; reaction time, 2 h.

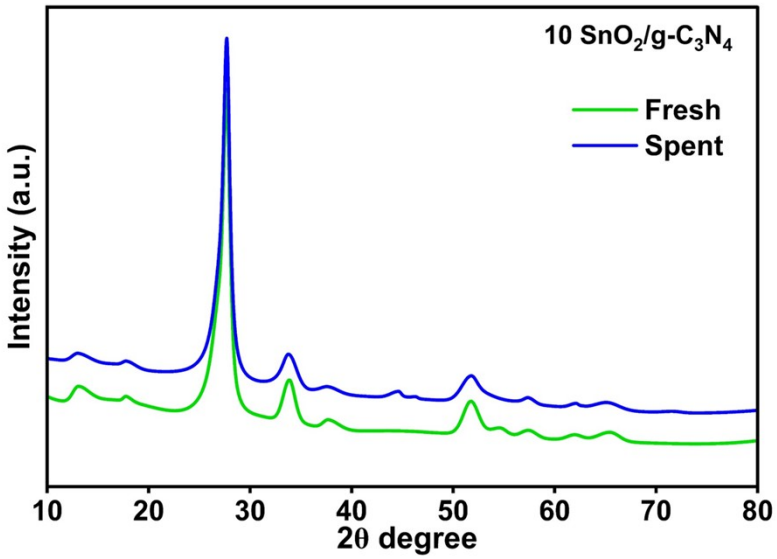

Figure S13 PXRD patterns of the 10 SnO_2/g-C_3N_4 before and after 4th cycle.

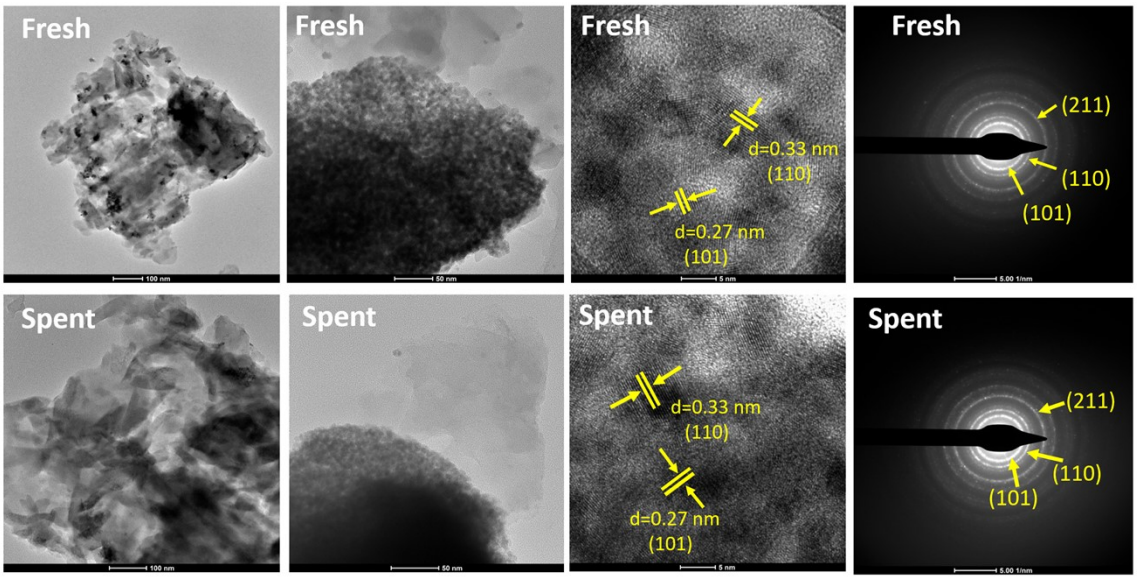

Figure S14 TEM, HRTEM and SAED pattern of 10 SnO_2/g-C_3N_4 fresh and spent catalyst after 4th cycle.

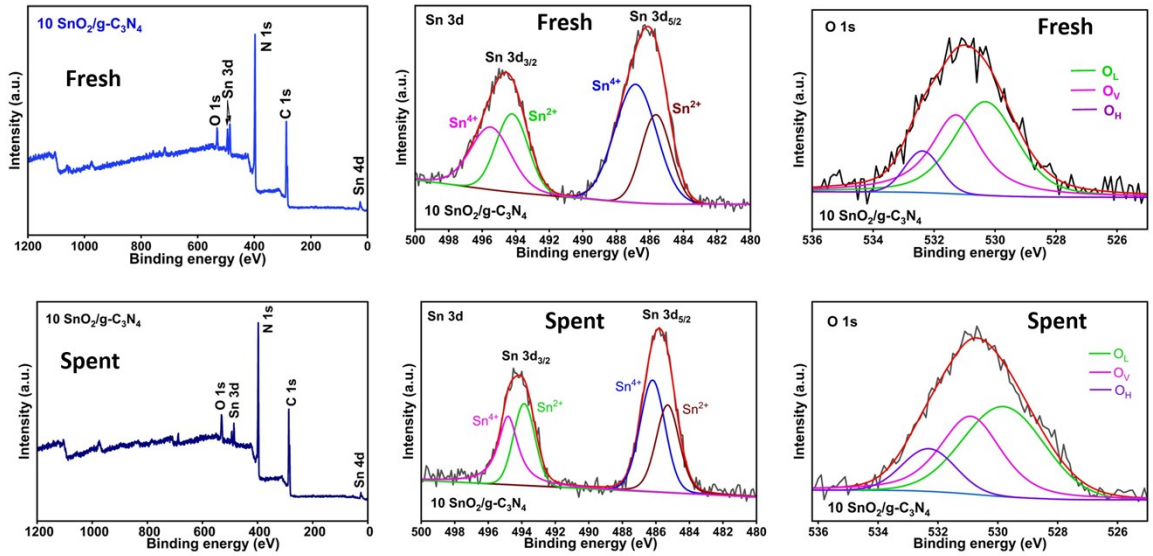

Figure S15 XPS spectra of the 10 SnO_2/g-C_3N_4 fresh and spent catalyst after 4th cycle.

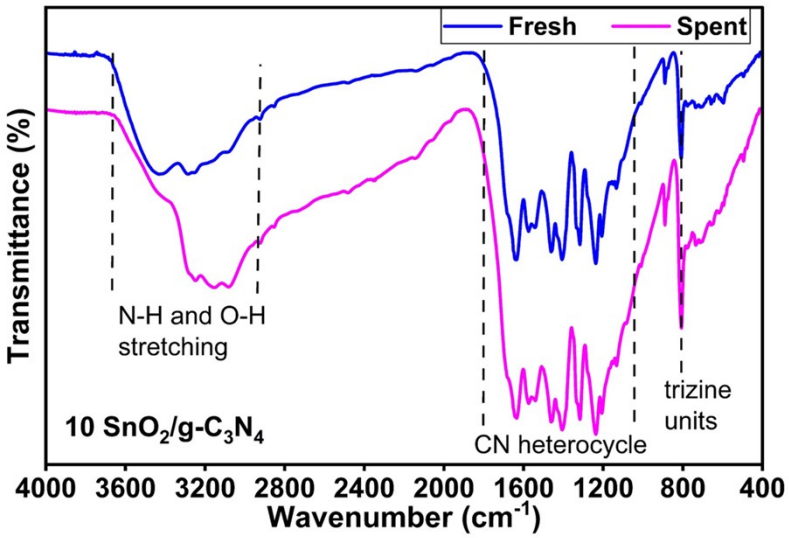

Figure S16 FTIR spectra of the 10 SnO_2/g-C_3N_4 fresh and spent catalyst after 4th cycle.

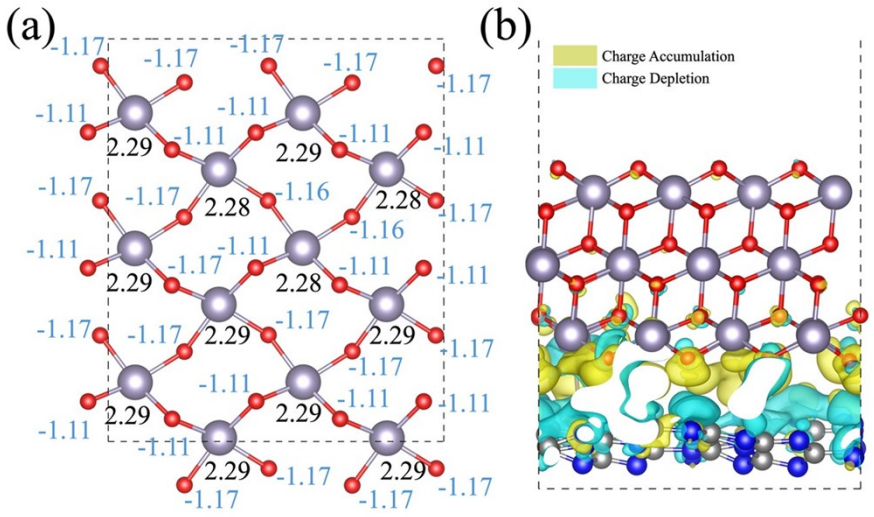

Figure S17 (a) Charges on atoms in the topmost surface layer and (b) charge density difference on the SnO_2/g-C_3N_4 surface.

Table S3 Comparison results of synthesis of ethylene urea (EU) from ethylenediamine (EDA) and ethylenediamine carbamate (EDA-CA).

Entry	Catalyst	Condition	Surface Area (m^2/g)	Acidity (mmol/g)	Basicity (mmol/g)	Reactor type	Temp (°C)	Time (h)	CO_2 (MPa)	Conv. (%)	Yield. (%)	Ref.
1	None	EDA: 1.0 mmol mL^{-1}, Catalyst free. Solvent free.	-	-	-	Batch	180	24	10	97	97	16
2	CeO_2	EDA: 2 mmol, Catalyst: 75 mg, Ethanol: 35 mmol	-	-	-	Batch	160	8	0.7	-	37	17
3	CeO_2	EDA: (10 mmol), Catalyst: 0.34 g, 2-Propanol: 200 mmol.	78	-	-	Batch	160	12	0.5	97	96	18
4	2.40ZnO/0.49KF/Al_2O_3	20 mmol of amine, 10 Catalyst: wt.% w.r.t amine, Methanol: 3.2 g	113.4	230	130	Batch	180	4	1	96	86	19
5	MOF-derived CeO_2	EDA: 10 mmol, Catalyst: 200 mg, Isopropanol: 200 mmol	147	24.94	88.96	Batch	160	12	0.5	95	94	20
6	CeO_2	EDA-CA: 2.08 g, Catalyst: 0.34 g, 2- propanol: 15 mL	60	-	-	Batch	140	24	-	83	83	21
7	Silica-supported IL	EDA: 5.0 mmol, Catalyst: 20 mg, Solvent free	254	-	-	Batch	100	12	2.5	98	94	22
8	CeO_2	F_{EDA-CA} = 0.57 mmol h^{-1}, F_{Sol} = 0.42 mL h^{-1}, CeO_2 2.0 g, W_{Cat}/F_{EDA-CA} = 3.48 g h $mmol^{-1.}$	86	94	52	Flow	90	72	-	99	93	23
9	Zr-doped CeO_2	EDA: 0.6 g, Catalyst 0.2 g, Isopropanol: 19.6 g.	119	-	4390	Batch	160	3	0.6	91.5	91.5	24
10	**10 SnO_2/g-C_3N_4**	**EDA: 0.1 mol, Catalyst: 250 mg, methanol: 80 ml.**	142	295	480	**Batch**	**160**	**2**	**2.5**	**95**	**94**	**This work**

References

1. R. Khan, S. S. Ahmad, H. Ihsan, S. S. Nadeem, S. Zulfiqar and F. A. A. Nugroho, *RSC Adv.*, 2025, **15**, 26776–26786.
2. V. Salve, P. Agale, S. Balgude, S. Mardikar, S. Dhotre and P. More, *RSC Adv.*, 2025, **15**, 15651–15669.
3. A. Singha, K. Bhaduri, A. C. Kothari and B. Chowdhury, *Mol. Catal.*, 2022, **533**, 112800.
4. P. Giannozzi, O. Baseggio, P. Bonfà, D. Brunato, R. Car, I. Carnimeo, C. Cavazzoni, S. de Gironcoli, P. Delugas, F. Ferrari Ruffino, A. Ferretti, N. Marzari, I. Timrov, A. Urru and S. Baroni, *J. Chem. Phys.*, **152** (2020), 154105.
5. P. Giannozzi, S. Baroni, N. Bonini, M. Calandra, R. Car, C. Cavazzoni, D. Ceresoli, G. L. Chiarotti, M. Cococcioni, I. Dabo, A. D. Corso, S. de Gironcoli, S. Fabris, G. Fratesi, R. Gebauer, U. Gerstmann, C. Gougoussis, A. Kokalj, M. Lazzeri, L. Martin-Samos, N. Marzari, F. Mauri, R. Mazzarello, S. Paolini, A. Pasquarello, L. Paulatto, C. Sbraccia, S. Scandolo, G. Sclauzero, A. P. Seitsonen, A. Smogunov, P. Umari and R. M. Wentzcovitch, *J. Phys.: Condens. Matter*, **21** (2009), 395502.

6. P. Giannozzi, O. Andreussi, T. Brumme, O. Bunau, M. B. Nardelli, M. Calandra, R. Car, C. Cavazzoni, D. Ceresoli, M. Cococcioni, N. Colonna, I. Carnimeo, A. D. Corso, S. de Gironcoli, P. Delugas, R. A. DiStasio, A. Ferretti, A. Floris, G. Fratesi, G. Fugallo, R. Gebauer, U. Gerstmann, F. Giustino, T. Gorni, J. Jia, M. Kawamura, H.-Y. Ko, A. Kokalj, E. Küçükbenli, M. Lazzeri, M. Marsili, N. Marzari, F. Mauri, N. L. Nguyen, H.-V. Nguyen, A. Otero-de-la-Roza, L. Paulatto, S. Poncé, D. Rocca, R. Sabatini, B. Santra, M. Schlipf, A. P. Seitsonen, A. Smogunov, I. Timrov, T. Thonhauser, P. Umari, N. Vast, X. Wu and S. Baroni, *J. Phys.: Condens. Matter*, **29** (2017), 465901.
7. J. P. Perdew, K. Burke and M. Ernzerhof, *Phys. Rev. Lett.*, **77** (1996), 3865–3868.
8. H. J. Monkhorst and J. D. Pack, *Phys. Rev. B*, **13** (1976), 5188–5192.
9. S. Grimme, J. Antony, S. Ehrlich and H. Krieg, *J. Chem. Phys.*, **132** (2010), 154104.
10. S. Grimme, S. Ehrlich and L. Goerigk, *J. Comput. Chem.*, **32** (2011), 1456–1465.
11. A. Iqbal, A. Tripathi and R. Thapa, *Inorg. Chem.*, **63** (2024), 1462–1470.
12. S. Kapse, S. Narasimhan and R. Thapa, *Chem. Sci.*, **13** (2022), 10003–10010.
13. S. Kumar and R. B. Choudhary, *J. Inorg. Organomet. Polym.*, 2023, **33**, 599–610.
14. W. Yu, D. Xu and T. Peng, J. *Mater. Chem. A,* 2015, **3**, 19936–19947.
15. B. Chowdhury, A.S. Rane, and A. Singha. *Development of Catalyst for synthesis of cyclic urea by CO_2 fixation*. Indian Patent Application No.: 202331045425, filed June 6, 2023 (Unpublished).
16. C. Wu, H. Cheng, R. Liu, Q. Wang, Y. Hao, Y. Yu and F. Zhao, *Green Chem*., 2010, **12**, 1811–1817.
17. A. Primo, E. Aguado and H. Garcia, *ChemCatChem,* 2013, **5**, 1020–1023.
18. M. Tamura, K. Noro, M. Honda, Y. Nakagawa and K. Tomishige, *Green Chem.*, 2013, **15**, 1567–1572.
19. N. Kulal, C. John and G. V. Shanbhag, *Appl. Catal. A: Gen.*, 2020, **598**, 117550.
20. G. S. More and R. Srivastava, *Ind. Eng. Chem. Res.*, 2021, **60**, 12492–12504.
21. J. Peng, M. Tamura, M. Yabushita, R. Fujii, Y. Nakagawa and K. Tomishige, *ACS Omega*, 2021, **6**, 27527–27535.
22. Q. Min, P. Miao, J. Liu, J. Ma, M. Qi and F. Shamsa, *Catal. Lett.*, 2022, **152**, 1476–1487.
23. R. Fujii, M. Yabushita, D. Asada, M. Tamura, Y. Nakagawa, A. Takahashi, A. Nakayama and K. Tomishige, *ACS Catal.*, 2023, **13**, 1562–1573.
24. F. Wang, Y. Jin, Y. Xue, L. Cui, S. Yu, N. Liu, Q. Ma, J. Xu and B. Xue, *Res. Chem. Intermed.*, 2024, **50**, 2175–2186.